In situ measurement of MEMS topography based on phase-shifting interferometry

Xi Chen
Hua Rong

In situ measurement of MEMS topography based on phase-shifting interferometry

Xi Chen and Hua Rong*
Nanjing Normal University, Jiangsu Province Key Laboratory of Optoelectronic Technology, No. 1 Wenyuan Road, Qixia District, Nanjing 210023, China

Abstract. Currently, phase-shifting interferometry is widely used in MEMS (micro-electro-mechanical system) microsurface topography measurements, and an expensive and high-precision piezoelectric transducer (PZT) is often necessary to realize phase-shift operation. Because of the feature of a MEMS structure which always has a flat substrate, a practical algorithm to calculate phase shifts by fast Fourier transformation (FFT) from gathered interference fringes of the substrate is presented, then microsurface topography can be reconstructed according to the obtained phase shifts. By means of the presented algorithm, an expensive and high-precision PZT is unnecessary and the phase-shift operation can even be carried out by rotating the fine focus adjustment knob. The accuracy and feasibility of the method have been verified by experiments. Experiments indicated that the presented method can satisfy the needs of *in situ* MEMS topography measurements and is very simple.
© The Authors. Published by SPIE under a Creative Commons Attribution 3.0 Unported License. Distribution or reproduction of this work in whole or in part requires full attribution of the original publication, including its DOI. [DOI: 10.1117/1.OE.54.2.024103]

1 Introduction

With the development of micro fabrication technology, accurate and simple three-dimensional MEMS surface topography metrology is becoming an urgent necessity.[1] Because of the advantages of noncontact and high-precision, optical metrology[2,3] has been widely applied in microsurface topography measurements such as phase-shifting interferometry(PSI),[4–8] white light interferometry,[9,10] heterodyne interferometry,[11,12] phase-locked interferometry,[13] and holography.[14,15] Among these, PSI plays a very important role. In many earlier phase extraction algorithms that were based on PSI, such as the Carré algorithm,[4] Stoilov algorithm,[6] Schwider algorithm,[7] and Hariharan algorithm,[8] one had to know the amount of each shift with a high accuracy to reduce the effects of phase-shift errors; therefore, it usually required a high-precision phase-shifter which is very expensive.[16] Meanwhile, on the assumption that only linear error exists in a phase shifter, a self-calibration algorithm was suggested by Carré[4] and developed by Morgan[17] and others. In this paper, based on the feature of MEMS structure which always has a plane substrate, a practical algorithm to calculate phase shifts from the gathered interference fringes of the substrate is presented, then microsurface topography can be reconstructed according to the obtained phase shifts. By means of the presented algorithm, an expensive and high-precision phase shifter is unnecessary and the phase-shift operation can even be carried out by rotating the fine focus adjustment knob. Obviously, it is useful for *in situ* MEMS topography measurement.

2 Principle

2.1 *Phase-Shift Calculation*

Figure 1 is a configuration of phase-shifting interferometry in which a piezoelectric transducer (PZT) is often used to move a reference mirror to induce a phase shift. The interferometer separates source light so that it follows two independent paths, one of which includes a reference mirror and the other includes the object surface. The separated light beams then recombine and interfere, and finally are directed to a digital camera which can record the resultant light intensity of each interferogram. Moving reference mirror by PZT, a phase shift is induced and the optical path difference of the two separated light beams is changed. Similarly, another interferogram that contains intensity distribution can be recorded. The intensity located at pixel (x, y) of each interferogram can be expressed in the form

$$I(x, y) = I_0(x, y) + I_0(x, y) \cdot A \cos[\varphi(x, y) + \psi], \quad (1)$$

where I_0 is the background intensity, A is the modulation, $\varphi(x, y)$ is the phase to be determined, and ψ is initial phase value.

Usually, the substrate surface of a MEMS device is flat and smooth enough (in Fig. 1); therefore, the waveform of the interference intensity along any line on the substrate is a fine cosine function, as shown in Fig. 2.

Considering two interferograms of a MEMS device surface obtained by a phase shift, the intensities can be represented as

$$I_1(x, y) = I_0(x, y) + I_0(x, y) \cdot A \cos[\varphi(x, y) + \psi_1], \quad (2)$$

$$I_2(x, y) = I_0(x, y) + I_0(x, y) \cdot A \cos[\varphi(x, y) + \psi_2]. \quad (3)$$

Along a line on the substrate, interference intensities of the two interferograms are cosine functions with the same period, as shown in Fig. 3. The initial phase values ψ_1, ψ_2 can be calculated by fast Fourier transformation (FFT).[18,19] The phase shift $\Delta \psi_{21}$ can be defined as

*Address all correspondence to: Hua Rong, E-mail: ronghua_1965@263.net

Fig. 1 A configuration of phase-shifting interferometry.

Fig. 3 Interference intensities of two interferograms on the substrate.
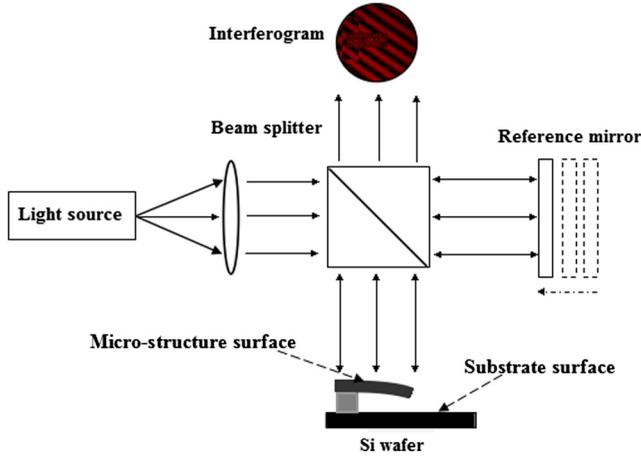
$$\Delta\psi_{21} = \psi_2 - \psi_1. \tag{4}$$

Obviously, $\Delta\psi_{21}$ is also the phase shift value of every pixel of the test surface.

where $\varphi(x, y)$ is the phase to be determined, and ψ_1, ψ_2, ψ_3, ψ_4, and ψ_5 are the initial phase values of the five interferograms, respectively.

Note that $\psi_2 = \psi_1 + \Delta\psi_{21}$, $\psi_3 = \psi_1 + \Delta\psi_{31}$, $\psi_4 = \psi_1 + \Delta\psi_{41}$ and $\psi_5 = \psi_1 + \Delta\psi_{51}$. Thus, Eqs. (5) to (9) can be rewritten as

$$I_1(x, y) = I_0(x, y) + I_0(x, y) \cdot A \cos[\varphi(x, y) + \psi_1], \tag{10}$$

2.2 Algorithm of Phase Distribution

Computing the phase distribution $\varphi(x, y)$ requires at least three interferograms. Existing literature[6] has shown that increasing the number of interferograms can appropriately improve the accuracy of surface topography measurements. A five-step algorithm is given as

$$I_1(x, y) = I_0(x, y) + I_0(x, y) \cdot A \cos[\varphi(x, y) + \psi_1], \tag{5}$$

$$I_2(x, y) = I_0(x, y) + I_0(x, y) \cdot A \cos[\varphi(x, y) + \psi_2], \tag{6}$$

$$I_3(x, y) = I_0(x, y) + I_0(x, y) \cdot A \cos[\varphi(x, y) + \psi_3], \tag{7}$$

$$I_4(x, y) = I_0(x, y) + I_0(x, y) \cdot A \cos[\varphi(x, y) + \psi_4], \tag{8}$$

$$I_5(x, y) = I_0(x, y) + I_0(x, y) \cdot A \cos[\varphi(x, y) + \psi_5], \tag{9}$$

$$I_2(x, y) = I_0(x, y) + I_0(x, y) \cdot A \cos[\varphi(x, y) + \psi_1 + \Delta\psi_{21}], \tag{11}$$

$$I_3(x, y) = I_0(x, y) + I_0(x, y) \cdot A \cos[\varphi(x, y) + \psi_1 + \Delta\psi_{31}], \tag{12}$$

$$I_4(x, y) = I_0(x, y) + I_0(x, y) \cdot A \cos[\varphi(x, y) + \psi_1 + \Delta\psi_{41}], \tag{13}$$

$$I_5(x, y) = I_0(x, y) + I_0(x, y) \cdot A \cos[\varphi(x, y) + \psi_1 + \Delta\psi_{51}]. \tag{14}$$

Now, in order to eliminate the parameter I_0, the intensity difference can be represented as

$$
\begin{aligned}
I_4(x, &y) - I_2(x, y) \\
&= I_0(x, y) \cdot A\{\cos[\varphi(x, y) + \psi_1 + \Delta\psi_{41}] \\
&\quad - \cos[\varphi(x, y) + \psi_1 + \Delta\psi_{21}]\} \\
&= -2I_0(x, y) \cdot A \left[\sin \frac{2\varphi(x, y) + 2\psi_1 + \Delta\psi_{41} + \Delta\psi_{21}}{2} \right. \\
&\quad \left. \cdot \sin \frac{\Delta\psi_{41} - \Delta\psi_{21}}{2} \right],
\end{aligned} \tag{15}
$$

Fig. 2 Waveform of the interference intensity on the substrate.

$$2I_3(x, y) - I_5(x, y) - I_1(x, y)$$
$$= I_0(x, y) \cdot A\{\cos[\varphi(x, y) + \psi_1 + \Delta\psi_{31}]$$
$$\quad - \cos[\varphi(x, y) + \psi_1 + \Delta\psi_{51}]\}$$
$$\quad + I_0(x, y) \cdot A\{\cos[\varphi(x, y) + \psi_1 + \Delta\psi_{31}]$$
$$\quad - \cos[\varphi(x, y) + \psi_1]\}$$
$$= -2I_0(x, y) \cdot A\left[\sin\frac{2\varphi(x, y) + 2\psi_1 + \Delta\psi_{31} + \Delta\psi_{51}}{2}\right.$$
$$\quad \left.\cdot \sin\frac{\Delta\psi_{31} - \Delta\psi_{51}}{2}\right]$$
$$\quad - 2I_0(x, y) \cdot A\left[\sin\frac{2\varphi(x, y) + 2\psi_1 + \Delta\psi_{31}}{2} \cdot \sin\frac{\Delta\psi_{31}}{2}\right].$$
(16)

From Eqs. (15) and (16), we figure out the following equation

$$\frac{2[I_4(x, y) - I_2(x, y)]}{2I_3(x, y) - I_5(x, y) - I_1(x, y)}$$
$$= \frac{2F \cdot \sin\frac{2\varphi(x,y) + 2\psi_1 + \Delta\psi_{41} + \Delta\psi_{21}}{2}}{P \cdot \sin\frac{2\varphi(x,y) + 2\psi_1 + \Delta\psi_{31} + \Delta\psi_{51}}{2} + Q \cdot \sin\frac{2\varphi(x,y) + 2\psi_1 + \Delta\psi_{31}}{2}},$$
(17)

where $F = \sin\frac{\Delta\psi_{41} - \Delta\psi_{21}}{2}$, $P = \sin\frac{\Delta\psi_{31} - \Delta\psi_{51}}{2}$, $Q = \sin\frac{\Delta\psi_{31}}{2}$

$$E = \frac{2(I_4 - I_2)}{2I_3 - I_5 - I_1}.$$

Thus, Eq. (17) can be rewritten as

$$EP \sin\left[\varphi(x, y) + \psi_1 + \frac{\Delta\psi_{31} + \Delta\psi_{51}}{2}\right]$$
$$\quad + EQ \sin\left[\varphi(x, y) + \psi_1 + \frac{\Delta\psi_{31}}{2}\right]$$
$$= 2F \sin\left[\varphi(x, y) + \psi_1 + \frac{\Delta\psi_{41} + \Delta\psi_{21}}{2}\right].$$
(18)

Fig. 4 Experimental setup.

Then further simplify Eq. (18) and the following two equations are obtained

$$\sin(\varphi(x, y) + \psi_1)\left[EP \cos\frac{\Delta\psi_{31} + \Delta\psi_{51}}{2} + EQ \cos\frac{\Delta\psi_{31}}{2}\right.$$
$$\quad \left. - 2F \cos\frac{\Delta\psi_{41} + \Delta\psi_{21}}{2}\right]$$
$$= \cos(\varphi(x, y) + \psi_1)\left[2F \sin\frac{\Delta\psi_{41} + \Delta\psi_{21}}{2}\right.$$
$$\quad \left. - EP \sin\frac{\Delta\psi_{31} + \Delta\psi_{51}}{2} - EQ \sin\frac{\Delta\psi_{31}}{2}\right],$$
(19)

$$\tan(\varphi(x, y) + \psi_1)$$
$$= -\frac{EP \sin\frac{\Delta\psi_{31} + \Delta\psi_{51}}{2} + EQ \sin\frac{\Delta\psi_{31}}{2} - 2F \sin\frac{\Delta\psi_{41} + \Delta\psi_{21}}{2}}{EP \cos\frac{\Delta\psi_{31} + \Delta\psi_{51}}{2} + EQ \cos\frac{\Delta\psi_{31}}{2} - 2F \cos\frac{\Delta\psi_{41} + \Delta\psi_{21}}{2}}.$$
(20)

Finally, the wavefront phase $\varphi(x, y) + \psi_1$ is obtained

$$\varphi(x, y) + \psi_1 = -\arctan\left(\frac{EP \sin\frac{\Delta\psi_{31} + \Delta\psi_{51}}{2} + EQ \sin\frac{\Delta\psi_{31}}{2} - 2F \sin\frac{\Delta\psi_{41} + \Delta\psi_{21}}{2}}{EP \cos\frac{\Delta\psi_{31} + \Delta\psi_{51}}{2} + EQ \cos\frac{\Delta\psi_{31}}{2} - 2F \cos\frac{\Delta\psi_{41} + \Delta\psi_{21}}{2}}\right)$$
(21)

where $\Delta\psi_{21}$, $\Delta\psi_{31}$, $\Delta\psi_{41}$ and $\Delta\psi_{51}$ are the phase shifts that can be calculated by the above mentioned method in Sec. 2.1.

The wavefront phase $\varphi(x, y) + \psi_1$ obtained from Eq. (21) is wrapped phase which is often discontinuous and needs to be unwrapped as a continuous phase distribution $\varphi'(x, y)$. Then, the microsurface topography is obtained by

$$h(x, y) = \frac{\lambda}{4\pi} \cdot \varphi'(x, y),$$
(22)

where λ is the light wavelength and $h(x, y)$ is a height function which relates to topography.

3 Experiment and Results

3.1 Experimental Setup

The experimental setup is a metallographic microscope (Type: Nikon-L150) whose objective is replaced by a Mirau interference objective (50×, Nikon), as shown in Figs. 4 and 5. The pixel size of the charge-coupled device (CCD) camera is 7.4 μm, and the pixel number is 2560 × 1920. The light
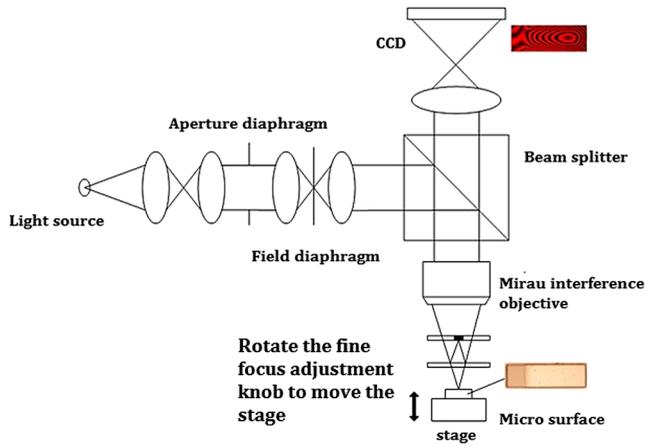
Fig. 5 Diagram of experimental system.

source wavelength is 633.3 nm. A micro structure, whose surface topography will be detected, is shown in Fig. 6. The detailed steps to record interferograms are as follows:

Step 1 Fix the micro structure on the stage, and adjust the microscope to show images of this micro structure clearly and make sure that there are interference fringes in the images.

Step 2 Rotate the fine focus adjustment knob slightly to move the stage and micro structure in the vertical direction. The optical path difference of two separated light beams is changed; therefore, another interferogram which is different from the former one can be recorded by CCD.
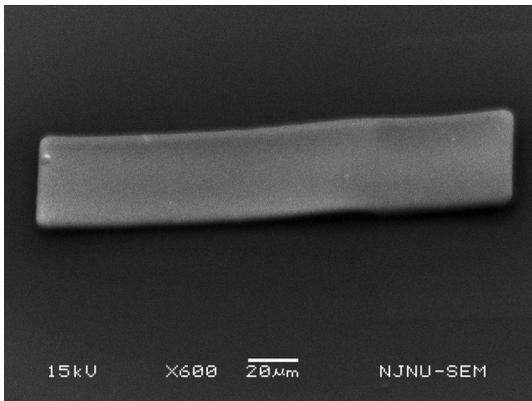
Fig. 6 A scanning electron microscope photo of the test sample.

Fig. 7 The first interferogram.
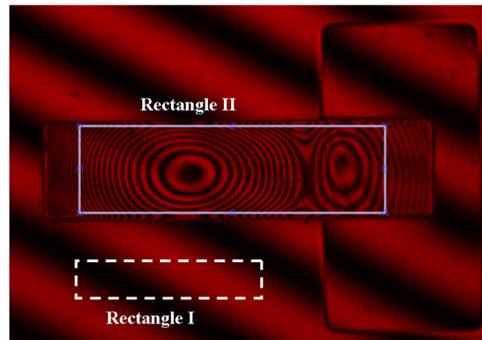
Fig. 8 The second interferogram.
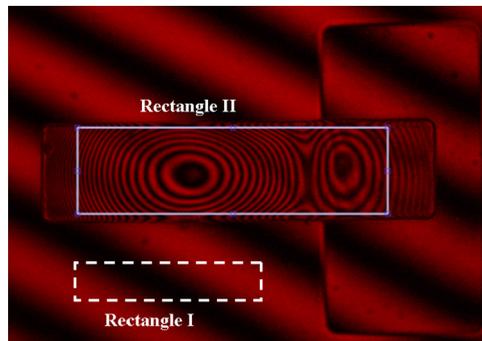
Fig. 9 The third interferogram.
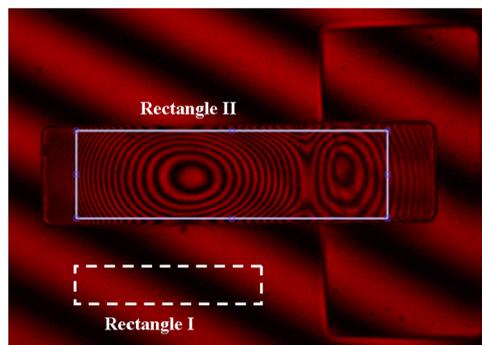
Fig. 10 The fourth interferogram.
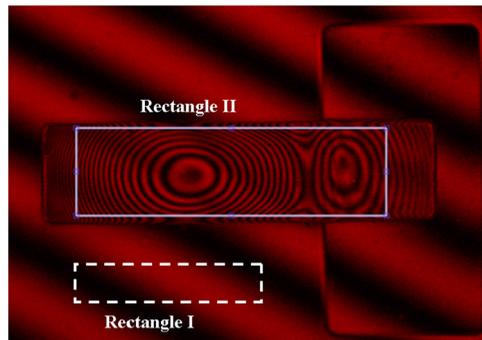
Fig. 11 The fifth interferogram.
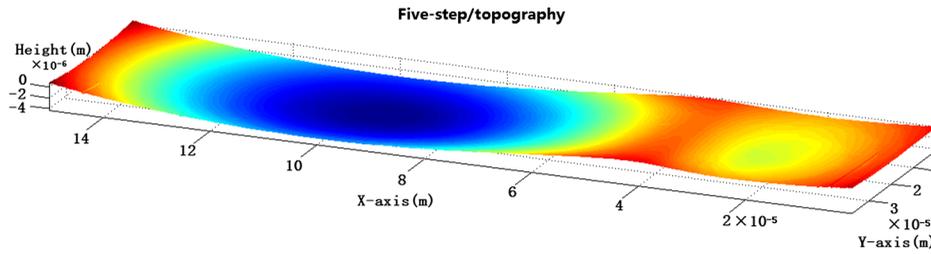
Fig. 12 Topography of the test surface (five-step).
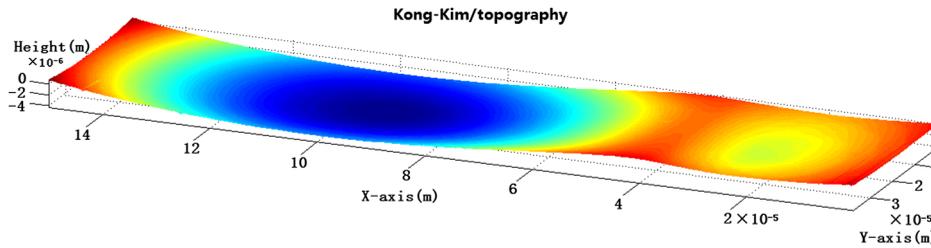
Fig. 13 Topography of the test surface (Kong-Kim).
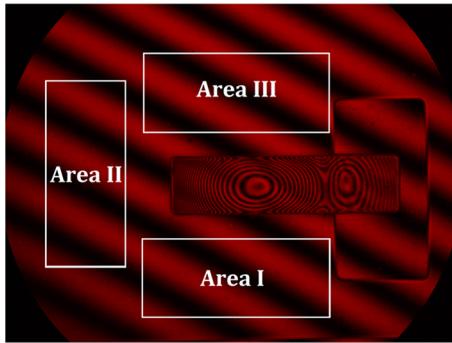
Fig. 14 Three different regions.
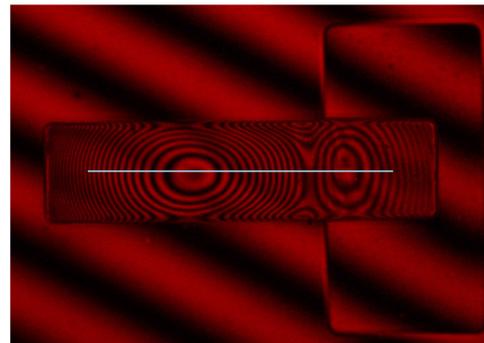
Fig. 15 A line on the test surface.

3.2 Topography Reconstruction

In order to reduce the influence of noise on the accuracy of the phase shift measurement, a rectangular region which contains many lines is selected (as shown in Figs. 7 through 11), then the average value of the phase shifts obtained from all lines in the rectangular region can be calculated and considered as the phase shift value of every pixel of the test surface; this is more accurate than that obtained from a single line.

On the substrate area, respectively, select five rectangular regions (i.e., Rectangle I) at the same position on the five interferograms, as shown in Figs. 7 through 11.

Using the above presented method, the actual phase shift values $\Delta\psi_{21}$, $\Delta\psi_{31}$, $\Delta\psi_{41}$ and $\Delta\psi_{51}$ also can be figured out by MATLAB®[20] as

Table 1 Error analysis of phase shift values.

	Area I			Area II			Area III		
	Presented method	Kong-Kim method	Δ_{A1}	Presented method	Kong-Kim method	Δ_{A2}	Presented method	Kong-Kim method	Δ_{A3}
$\Delta\psi_{21}$	58.40	57.08	1.32	58.56	58.26	0.30	58.57	58.95	0.38
$\Delta\psi_{31}$	132.78	131.40	1.38	131.89	131.79	0.10	132.23	132.30	0.07
$\Delta\psi_{41}$	213.85	208.74	5.11	213.18	210.98	2.20	213.38	212.79	0.59
$\Delta\psi_{51}$	16.70	16.88	0.18	16.41	16.39	0.02	16.72	16.85	0.13

$\Delta \psi_{21} = 58.79$ deg $\Delta \psi_{31} = 132.47$ deg

$\Delta \psi_{41} = 213.37$ deg $\Delta \psi_{51} = 16.31$ deg.

Select the rectangular region (i.e., Rectangle II) in Figs. 7 through 11 as the test surface, then the test surface topography is reconstructed as shown in Fig. 12.

4 Discussion

The optical resolution of the microscope is 0.575 μm, and the actual length of a pixel is 0.15 μm in the horizontal direction while the resolution in the vertical direction is 0.62 nm. The measurement resolution in the vertical direction is often defined by practical experiments.

In the existing literature, In-bok Kong and Seung-Woo Kim presented a general algorithm of phase-shifting interferometry by iterative least-squares fitting[18] which used the idea of iteration[21–23] and had a rather high precision in the phase shift and topography measurement.

Hence, the test surface topography, which is also mentioned in Sec. 3.2 and is reconstructed by the Kong-Kim algorithm, is given here, as shown in Fig. 13.
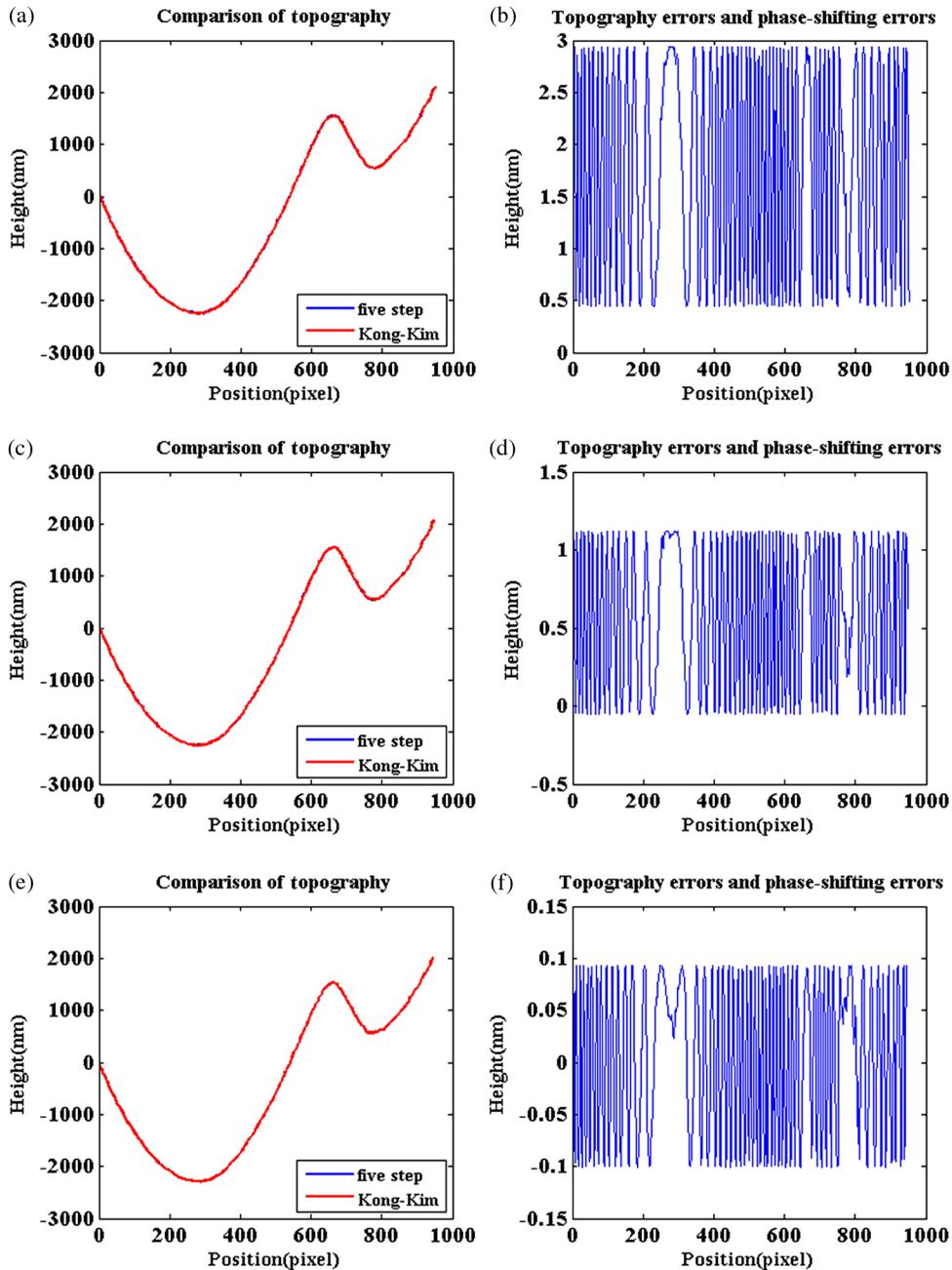
Fig. 16 Reconstructed topography and topography errors by three sets of phase shift values: (a) topography reconstructed by the calculated phase shift values in Area I; (b) relationships between topography errors and the calculated phase shift values in Area I; (c) topography reconstructed by the calculated phase shift values in Area II; (d) relationships between topography errors and the calculated phase shift values in Area II; (e) topography reconstructed by the calculated phase shift values in Area III; (f) relationships between topography errors and the calculated phase shift values in Area III.
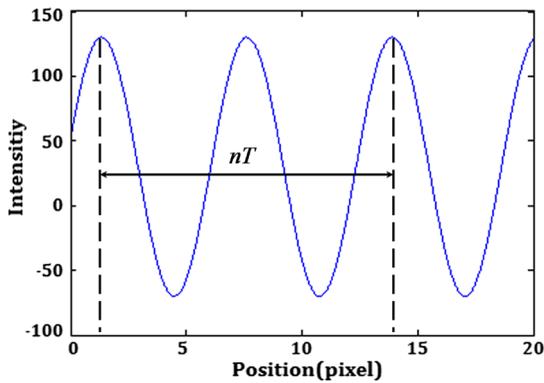
Fig. 17 Waveform of the interference intensity on the substrate.

Fig. 18 Illustration: how to select complete periodic waveforms.

From Figs. 12 to 13, it shows that the test surface topography which is reconstructed by the presented method is consistent with the reconstructed topography by the Kong-Kim algorithm.

Meanwhile, the resulted phase shift values in the Kong-Kim algorithm can be compared with the calculated phase shift values in the presented method.

Select three different regions in Fig. 14 on five corresponding interferograms (Figs. 7 through 11), then three sets of results which are obtained by, respectively, processing three regions of the interferograms as can be seen in Table 1.

In Table 1, Δ_{A1}, Δ_{A2}, and Δ_{A3} are the absolute errors between the presented method (Five-step) and the Kong-Kim algorithm. From Table 1 and Fig. 14, we can see that whatever is images in Area I, Area II, or Area III, the absolute errors are very small. Especially in Area III where the light intensity is stronger, the absolute error Δ_{A3} is minimal among the three different regions mostly because it has a better signal-to-noise ratio. Moreover, in theory, the phase shift values are the same whatever is present in Area I, Area II, or Area III because the phase shifts are global. From Table 1, it is clear that the phase shift values which are calculated by the presented method are also nearly consistent. Thus, compared with Kong-Kim algorithm, the results from the presented method are better in the region where the light intensity is weaker (i.e., Area I and Area II), and the main reason is the presented method which is based on FFT can filter some noise in the phase-shift calculation and improve the precision of phase-shift calculation. Therefore, to obtain accurate phase shift values, it is necessary to process the good-quality regions of the obtained interferograms as far as possible.[8,24]

In order to evaluate the influence of the phase-shifting errors, we respectively adopt three sets of calculated phase shift values in Table 1 to reconstruct topography by processing a line in Fig. 15, and the results are shown in Fig. 16.

In Figs. 16(a), 16(c) and 16(e), it is clear that the results of topography which are reconstructed by using three sets of phase shift values in Table 1 are extremely overlapping. Since the phase-shifting error is minimal in Area III, the corresponding topography error also has a minimal value, which is about 0.1 nm, as shown in Fig. 16(f). Besides, the phase-shifting error is larger in Area I; therefore, the corresponding topography error has a bigger value which is about 3 nm, as shown in Fig. 16(b).

In order to further improve the accuracy of the phase shift values, the initial phase ψ should be precisely figured out as far as possible. As shown in Fig. 17, considering the feature
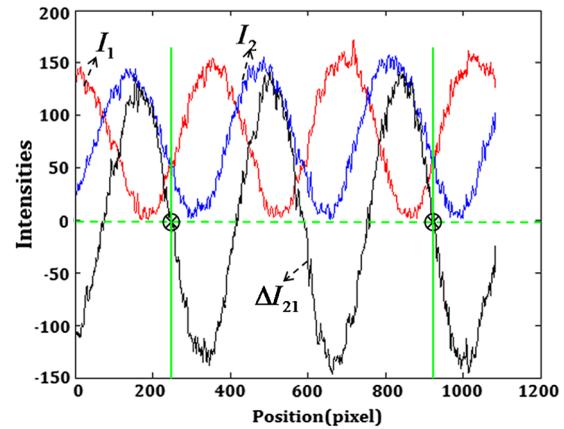
of FFT, it is better to select n complete periodic waveforms on the substrate.

The method to select n complete periodic waveforms is as follows:

Step 1 Calculate the interference intensity difference along a line $\Delta I_{21} = I_2 - I_1 = -2I_0 \cdot A \sin\frac{\varphi_2 - \varphi_1}{2} \sin[\varphi(x,y) + \frac{\varphi_2 + \varphi_1}{2}]$, and the period of ΔI_{21} is the same as I_1 and I_2, as shown in Fig. 18.

Step 2 Figure out a couple of zero points of ΔI_{21} by MATLAB, and make sure that the length between the two zero points includes a few of the complete periodic waveforms.

Step 3 Select a section on I_1 and I_2 respectively, between the two zero points of ΔI_{21} to calculate phase shift $\Delta \psi_{21}$, as shown in Fig. 18.

The above-mentioned phase shift values are the pivotal factor that influences the presented algorithm. Additionally, there are some other error sources of the proposed method as follows:

1. The instability of the light source causes noises in the illuminated field.
2. The ambient vibration affects the process of image capture.
3. The optical defocus affects the quality of interferograms in practical experiments.
4. In many cases, the CCD is nonlinear so that it also induces measurement errors.

5 Conclusion

The accuracy and feasibility of the method have been verified by experiments. The main advantages of the presented algorithm are as follows: (1) the algorithm can meet the accuracy requirement of the vast majority of MEMS topography measurements. (2) The speed of computation is faster than the iteration operation and initial values are unnecessary while inappropriate initial values can even lead to wrong results. (3) The phase-shift calculation is simple and the phase-shift operation does not require a high-precision PZT, just rotation of the fine focus adjustment knob; therefore, it makes the presented method more practical and meaningful.

In a word, it is very suitable for *in situ* MEMS topography measurements.

References

1. L. D. Chiffre et al., "Surfaces in precision engineering, micro-engineering and nanotechnology," *Ann. CIRP* **52**(2), 561–577 (2003).
2. D. Malacara, *Optical Shop Testing*, 3rd ed., John Wiley & Sons, New York (2007).
3. J. C. Wyant, "Computerized interferometric surface measurements," *Appl. Opt.* **52**(1), 1–8 (2013).
4. P. Carré, "Installation et utilisation du comparateur photoélectrique et interférentiel du Bureau International des Poids et Mesures," *Metrologia* **2**(1), 13–23 (1966).
5. B. Bhushan, J. C. Wyant, and C. L. Koliopoulos, "Measurement of surface topography of magnetic tapes by Mirau interferometry," *Appl. Opt.* **24**(10), 1489–1497 (1985).
6. G. Stoilov and T. Drgaostinov, "Phase-stepping interferometry: five frame algorithm with an arbitrary step," *Opt. Laser Eng.* **28**(1), 61–69 (1997).
7. J. Schwider et al., "Digital wave-front measuring interferometry: some systematic error sources," *Appl. Opt.* **22**(21), 3421–3432 (1983).
8. P. Hariharan, B. F. Oreb, and T. Eiju, "Digital phase-shifting interferometry: a simple error-compensating phase calculation algorithm," *Appl. Opt.* **26**(13), 2504–2506 (1987).
9. L. C. Chen, M. T. Le, and Y. S. Lin, "3-D micro surface profilometry employing novel Mirau-based lateral scanning interferometry," *Meas. Sci. Technol.* **25**(9), 094004 (2014).
10. J. C. Wyant, "White light interferometry," *Proc. SPIE* **4737**, 98–107 (2002).
11. J. E. Greivenkamp, "Generalized data reduction for heterodyne interferometry," *Opt. Eng.* **23**(4), 350–352 (1984).
12. T. Schuldt et al., "Picometre and nanoradian heterodyne interferometry and its application in dilatometry and surface metrology," *Meas. Sci. Technol.* **23**(5), 054008 (2012).
13. G. W. Johnson, D. C. Leiner, and D. T. Moore, "Phase-locked interferometry," *Opt. Eng.* **18**(1), 180146 (1979).
14. W. Chen et al., "Quantitative detection and compensation of phase-shifting error in two-step phase-shifting digital holography," *Opt. Commun.* **282**(14), 2800–2805 (2009).
15. W. Chen and X. D. Chen, "Quantitative phase retrieval of a complex-valued object using variable function orders in the fractional Fourier domain," *Opt. Express* **18**(13), 13536–13541 (2010).
16. R. Langoju, A. Patil, and P. Rastogi, "Statistical study of generalized nonlinear phase step estimation methods in phase-shifting interferometry," *Appl. Opt.* **46**(33), 8007–8014 (2007).
17. C. J. Morgan, "Least-squares estimation in phase-measurement interferometry," *Opt. Lett.* **7**(8), 368–370 (1982).
18. M. Takeda, H. Ina, and S. Kobayashi, "Fourier-transform method of fringe-pattern analysis for computer-based topography and interferometry," *J. Opt. Soc. Am.* **72**(1), 156–160 (1982).
19. K. A. Goldberg and J. Bokor, "Fourier-transform method of phase-shift determination," *Appl. Opt.* **40**(17), 2886–2894 (2001).
20. R. C. Gonzalez, *Digital Image Processing Using MATLAB*, Prentice Hall, New Jersey (2003).
21. I. B. Kong and S. W. Kim, "General algorithm of phase-shifting interferometry by iterative least-squares fitting," *Opt. Eng.* **34**(1), 183–188 (1995).
22. H. W. Guo and M. Y. Chen, "Least-squares algorithm for phase-stepping interferometry with an unknown relative step," *Appl. Opt.* **44**(23), 4854–4859 (2005).
23. Y. Joonho and J. K. Nam, "Minimization of spectral phase errors in spectrally resolved white light interferometry by the iterative least-squared phase-shifting method," *Meas. Sci. Technol.* **23**(12), 125203 (2012).
24. Y. Surrel, "Additive noise effect in digital phase detection," *Appl. Opt.* **36**(1), 271–276 (1997).

Xi Chen is pursuing his MS degree at Nanjing Normal University. In 2012, he graduated with a BS degree in electrical engineering. His current research interests include micro-electro-mechanical systems (MEMS) and optical engineering.

Hua Rong is an associate professor at Nanjing Normal University. He received his BS and MS degrees from Xi'an Jiaotong University, China, in 1988 and 1999, respectively, and his PhD degree from Southeast University, China, in 2004, all in electrical engineering. His current research interests include micro-electro-mechanical systems (MEMS) and optical engineering.